8-1-2004

Unified theory of the ab-plane and c-axis penetration depths of underdoped cuprates

Daniel E. Sheehy
The University of British Columbia

T. P. Davis
The University of British Columbia

M. Franz
The University of British Columbia

Recommended Citation

Sheehy, D., Davis, T., & Franz, M. (2004). Unified theory of the ab-plane and c-axis penetration depths of underdoped cuprates. *Physical Review B - Condensed Matter and Materials Physics, 70* (5) https://doi.org/10.1103/PhysRevB.70.054510

Nodal Protectorate: A Unified Theory of the ab-plane and c-axis Penetration Depths of Underdoped cuprates

Daniel E. Sheehy,* T.P. Davis, and M. Franz
Department of Physics and Astronomy, University of British Columbia, 6224 Agricultural Road, Vancouver, B.C. V6T1Z1, Canada
(Dated: February 8, 2020)

We formulate a model describing the doping (x) and temperature (T) dependence of the ab-plane and c-axis penetration depth of a cuprate superconductor. The model incorporates the suppression of the superfluid density with underdoping as the system approaches the Mott-Hubbard insulating state by augmenting a d-wave BCS model with a phenomenological charge renormalization factor that is vanishingly small for states away from the nodes of the d-wave pair potential but close to unity in the vicinity of the nodes. The c-axis penetration depth is captured within a model of incoherent electron tunneling between the CuO_2 planes. Application of this model to the recent experimental data on the high-purity single crystals of $YBa_2Cu_3O_{6+\delta}$ implies existence of a "nodal protectorate", a k-space region in the vicinity of the nodes whose size decreases in proportion to x, in which d-wave quasiparticles remain sharp even as the system teeters on the brink of becoming an insulator. The superfluid density, which is extremely small for these samples, also appears to come exclusively from these protected nodal regions.

I. INTRODUCTION

It is believed that to understand the high-T_c cuprate superconductors, one must understand the problem of doping a Mott insulator.[1] Conversely, understanding the manner in which superconducting order gives way to the antiferromagnetic insulator at half filling would provide important clues to the solution of this fundamental challenge.[2,3,4,5] Indeed, those cuprates which have the lowest concentrations x of dopants (so-called "underdoped" cuprates) possess many of the most enigmatic and mysterious experimental properties. In particular, as x is reduced, the zero-temperature pair-potential maximum Δ_0 *grows* while the zero-temperature superfluid stiffness $\rho_s(0)$ and transition temperature T_c *decrease*.[6] In addition, the underdoped cuprates possess a "pseudogap"[7] in the single-particle excitation spectrum that persists above T_c. Taken together, these suggest that the way superconductivity is destroyed as $x \to 0$ is very unusual. Unfortunately, there has been a paucity of data on such very underdoped cuprates, in part due to sample preparation difficulties. In addition, such materials are often very disordered, complicating analysis of their intrinsic physical properties. Recently, however, Liang *et al.*[8] have devised a way to vary x in the doping phase diagram for a single crystal of $YBa_2Cu_3O_{6+\delta}$ (YBCO) in an essentially continuous fashion. Briefly, their method utilizes the fact that the *effective* doping on the CuO_2 planes is governed by both the oxygen concentration and the degree of oxygen ordering in the CuO chains. By varying the latter variable (via room temperature annealing), these authors can alter the effective doping (and thus T_c) to explore the doping dependence of physical quantities (such as the c-axis penetration depth[9,10]) in the strongly underdoped regime $x \to 0$.

Motivated by the recent c-axis penetration results of Hosseini *et al.*,[9,10] in this Paper we develop a model aimed at capturing the overall phenomenology of the doping and temperature dependence of the ab-plane and c-axis penetration depths (λ_{ab} and λ_c, respectively). Our model combines incoherent tunneling in the c-direction with a phenomenological momentum-dependent charge renormalization factor inspired by the idea of Ioffe and Millis[11] to account for anomalous doping dependences. On a more fundamental level we are interested in understanding the constraints that this data imposes on the models of strongly correlated electron matter describing the d-wave superconductor on the verge of becoming a Mott-Hubbard insulator. Our results indicate that the appropriate effective theory must exhibit a "nodal protectorate" consisting of regions in the vicinity of the d-wave gap nodes where the quasiparticles remain well defined even as $x \to 0$.

To begin, let us review the overall phenomenology of the penetration depth in the cuprates. For the moment, we are interested in general trends (especially in the strongly underdoped regime $x \to 0$) in the penetration depth. To the extent that such data is available,[6,12,13] the ab-plane penetration depth $\lambda_{ab}(x,T)$ exhibits the following behavior:

$$\rho_s^{ab}(x,T) = \frac{\hbar^2 c^2 d}{16\pi e^2 \lambda_{ab}^2(x,T)} \simeq ax - bk_B T, \qquad (1)$$

where we have expressed $\lambda_{ab}(x,T)$ in terms of the associated superfluid stiffness $\rho_s^{ab}(x,T)$ measuring the free energy cost to a variation of the order-parameter phase in the ab plane. Here, d denotes the distance between copper-oxygen layers. For YBCO the relevant parameters are $a \simeq 244$meV and $b \simeq 3.0$.[12,14] We shall assume that this phenomenology holds for all underdoped cuprates[15,16]. The coefficient of T in Eq. (1) is *nearly* doping independent, in the sense that although it varies as the gap amplitude Δ_0 varies, it does not vary as strongly as $\rho_s^{ab}(x,0)$ i.e., linear in x. The T-linear term is well known and is understood to be due to the excitation of quasiparticles out of the condensate near the

nodes of the d-wave order parameter.[17] The fact that this relation holds to very low dopings (along with other experiments sensitive to nodal physics, see, e.g., Ref. [18]) indicates that near the nodes elementary excitations in cuprates are well described by conventional BCS quasiparticles even for $x \to 0$.

The doping dependence of $\rho_s^{ab}(x,T)$, on the other hand, represents one of the central mysteries in the cuprates.[14] The linear in x reduction of $\rho_s^{ab}(x,0)$ as one approaches half filling must be attributed to the proximity of the Mott-Hubbard insulating phase. However, most theoretical treatments (such as the RVB-type[19] and Gutzwiller projection[20,21] approaches) that can account for the observed x-dependence of $\rho_s^{ab}(x,0)$ also predict a strongly x-dependent prefactor b in Eq. (1), in disagreement with the data. Thus, the central theoretical problem appears to lie in constructing a model that would make only a small fraction $\sim x$ of all electrons participate in the superconducting condensate while at the same time preserve the simple BCS character of the nodal quasiparticles. In the following we resolve this problem by postulating that, at least for the purposes of studying the superfluid stiffness, the underdoped cuprates can be described by the BCS theory augmented with a phenomenological constraint that only Cooper pairs composed of electrons with momenta in the vicinity of the nodal points effectively couple to the external electromagnetic field. We implement this idea by extending the "effective charge renormalization" concept introduced in this context by Ioffe and Millis.[11]

This model, described in a more detail below, is *designed* to reproduce the ab-plane phenomenology embodied in Eq. (1). What makes us believe that it might be of more general validity is the fact that it also reproduces the doping dependence of the c-axis superfluid stiffness, $\rho_s^c(x,T)$, once we adopt a model for interlayer coupling that gives the correct (nonlinear) temperature dependence of this quantity. The phenomenology along the c-axis is tantalizingly similar to the ab plane case and can be written in the following way:[9,10,22,23]

$$\rho_s^c(x,T) \propto \lambda_c^{-2}(x,T) \simeq Ax^\alpha - BT^\alpha, \tag{2}$$

where the exponent α is, within the experimental accuracy, the same for both x and T and close to 2, while A, B are again x and T independent constants. The fact that the temperature dependence is nearly quadratic (as opposed to linear) points to the *incoherent* coupling between the copper-oxygen planes, as discussed by previous authors.[24,25] In the following we shall clarify the specific conditions under which such a nearly quadratic T-dependence arises for the incoherent tunneling model. More importantly we show that within our scheme for the effective charge the *same power law* also necessarily governs the doping dependence of $\rho_s^c(x,0)$, in agreement with Eq. (2).

This Paper is organized as follows: In Sec. II, we augment the standard BCS expression for λ_{ab} with a phenomenological charge renormalization factor. By appealing to experimental data, the parameters determining this factor are extracted. In Sec. III, we consider a tunneling model of c-axis transport and augment the resulting expression for λ_c with the same charge renormalization factor in an analagous way. It is shown that the T and x dependences of our expression for λ_c agree qualitatively (having made certain assumptions) with Eq. (2). In Sec. III, we fit our expression for λ_c to the results of Refs. 9,10). In Sec. V we make some concluding remarks. Certain calculational details are relegated to Appendices A amd B.

II. ab-PLANE PROPERTIES

The starting point of our calculation of the ab-plane penetration depth $\lambda_{ab}(T)$ is the following Hamiltonian for a d-wave superconductor coupled to an applied in-plane electromagnetic field:

$$\begin{aligned} H &= H_{\rm pair} + H_{\rm int}, \\ H_{\rm pair} &= \sum_{\mathbf{k},\sigma} \epsilon_{\mathbf{k}} c^\dagger_{\mathbf{k},\sigma} c_{\mathbf{k},\sigma} + \sum_k \Delta_{\mathbf{k}} (c^\dagger_{\mathbf{k},\uparrow} c^\dagger_{-\mathbf{k},\downarrow} + \text{h.c.}), \end{aligned} \tag{3}$$

where $H_{\rm pair}$ is the standard BCS pairing Hamiltonian with the single-particle energy $\epsilon_{\mathbf{k}} = -2t(\cos k_x a + \cos k_y a) - \mu$ with a the lattice spacing. The pair potential $\Delta_{\mathbf{k}} = \frac{1}{2}\Delta_0(\cos k_x a - \cos k_y a)$; we shall always assume that the maximum pair potential Δ_0 is approximately temperature independent. Here, $H_{\rm int}$ refers to additional interactions not captured by $H_{\rm pair}$ which describe the physics of the proximity to the Mott-Hubbard insulating phase at half filling. Our strategy will be to compute λ_{ab}^{-2} by first neglecting $H_{\rm int}$ and computing the usual BCS result for the superfluid density in a d-wave superconductor. Then, we shall include the residual interactions $H_{\rm int}$ via a phenomenological charge renormalization motivated by the work of Millis *et al.*[27] and Ioffe and Millis.[11] The calculation of the penetration depth for $H_{\rm pair}$ is standard and is presented in Appendix A for completeness. The final result may be expressed as

$$\begin{aligned} \frac{1}{\lambda_{ab}^2(x,T)} &= \frac{e^2 n}{d} \sum_{\mathbf{k}} Z_{\mathbf{k}}^2 \left(\frac{\partial \epsilon_{\mathbf{k}}}{\partial k_x} \right)^2 \frac{\Delta_{\mathbf{k}}^2}{E_{\mathbf{k}}^2} \\ &\quad \times \left[\frac{1}{E_{\mathbf{k}}} - \frac{\partial}{\partial E_{\mathbf{k}}} \right] \tanh \frac{1}{2} \beta E_{\mathbf{k}}, \end{aligned} \tag{4}$$

with $E_{\mathbf{k}} = \sqrt{\epsilon_{\mathbf{k}}^2 + \Delta_{\mathbf{k}}^2}$ the BCS d-wave excitation spectrum and $\beta = 1/T$ the inverse temperature. The factor $Z_{\mathbf{k}}^2$ will be discussed shortly.

We shall take Eq. (4) to be the starting point of our phenomenological analysis of the ab-plane penetration depth data. It contains a sum over all momentum vectors $\mathbf{k}$ in the Brillouin zone and has been cast into a form where the zero temperature value $\lambda_{ab}(0)^{-2}$ and the finite temperature correction $\delta\lambda_{ab}(T) \equiv \lambda_{ab}^{-2}(0) - \lambda_{ab}^{-2}(T)$ are treated on an equal footing; in particular they are

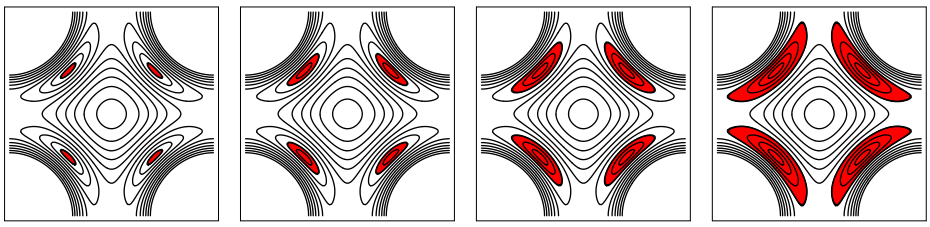

FIG. 1: Schematic plot of the assumed form for $Z_{\mathbf{k}}$, showing the "nodal protectorate" region (shading) of the Brillouin zone where states contribute to the formation of the condensate for a cuprate at a particular doping x. The black lines are the constant energy contours in the Brillouin zone (which do not vary with doping). Near optimal doping ($x = 20$), electrons in a large region around the node contribute to the Meissner response. As the doping is reduced this region is progressively reduced, leaving a small "patch" near the nodes where superconductivity remains robust. We remark that the c-axis penetration depth measurements of Ref. 10 were performed on extremely underdoped samples with effective dopings x that are approximately represented by the leftmost panel.

both dominated by the regions in the k-space close to the nodes of the d-wave gap function. As discussed in Appendix A, for $Z_{\mathbf{k}} = 1$ this expression is fully equivalent to well-known expressions for λ_{ab}^2 that have appeared previously in the literature.[28,29]

Following Ref. [11] we have introduced in Eq. (4) a phenomenological charge renormalization factor $Z_{\mathbf{k}}$ by means of the replacement

$$e^2 \sum_{\mathbf{k}} \rightarrow e^2 \sum_{\mathbf{k}} Z_{\mathbf{k}}^2. \tag{5}$$

This is done to incorporate the effects of the interactions contained in $H_{\rm int}$ responsible for the gradual demise of superconducting order as the Mott-Hubbard insulating phase is approached near the half filling. The main difference between our approach and that of Ref. [11] is that we have incorporated $Z_{\mathbf{k}}$ into the full expression for λ_{ab}^2, as opposed to the temperature dependent part only. This is in keeping with our philosophy of treating both components on the equal footing. At this stage we do not attempt to justify the inclusion of $Z_{\mathbf{k}}$ from microscopic considerations; we merely state that such charge renormalization is not prohibited by any general principle (and is known to occur e.g. in the Fermi liquid theory). We offer some discussion of the possible origins of $Z_{\mathbf{k}}$ in Sec. IV.

In the absence of a microscopic theory for $Z_{\mathbf{k}}$ we must rely on experimental data to infer the behavior of this quantity. We begin by reiterating that, in weak coupling BCS theory $Z_{\mathbf{k}} = 1$ and a direct evaluation of Eq. (4) yields a result which does not conform to the observed ab-plane phenomenology[14].

In particular BCS theory yields a correct linear-T dependence of $\delta\lambda_{ab}(T)$ but the wrong doping dependence of $\lambda_{ab}^{-2}(0)$, which would scale with the total number of electrons $(1 - x)$ in disagreement with Eq. (1). To rectify this discrepancy the form of $Z_{\mathbf{k}}$ must be modified. Since at low temperatures the T-dependence of $\delta\lambda_{ab}(T)$ comes from thermally excited quasiparticles near the four nodal points of a d-wave gap, it is clear that in order to preserve this correct temperature dependence $Z_{\mathbf{k}}$ must remain *close to unity* in the nodal regions. To suppress the overall magnitude of $\lambda_{ab}^{-2}(0)$ it then follows that $Z_{\mathbf{k}}$ must be small *outside the nodal regions*. In addition, to conform to the $\lambda_{ab}^{-2}(0) \sim x$ scaling the size of the "patch" in which $Z_{\mathbf{k}} \approx 1$ must scale with x.

The ab-plane phenomenology thus dictates the following form for the charge renormalization factor

$$Z_{\mathbf{k}} \approx \begin{cases} Z_0 & \text{for } E_{\mathbf{k}} < E_{\rm c}, \\ 0 & \text{for } E_{\mathbf{k}} > E_{\rm c}, \end{cases} \tag{6}$$

with Z_0 a constant of order 1 and $E_{\rm c} \sim x$ the characteristic cutoff energy that is chosen to obtain the correct magnitude of the zero-temperature superfluid stiffness. As illustrated in Fig. 1, this choice of $Z_{\mathbf{k}}$ effectively restricts the sum over the entire Brillouin zone in Eq. (4) to the immediate vicinity of the nodes. At low temperatures, such a choice affects the diamagnetic response (which is sensitive to the entire Fermi surface) but not the paramagnetic response which governs the temperature dependence.

To see how this reproduces the assumed phenomenology, we proceed by inserting the assumed form for $Z_{\mathbf{k}}$ into Eq. (4). We make an assumption, which we verify momentarily, that $E_{\rm c}$ is sufficiently small (i.e. $E_{\rm c} \ll \Delta_0$) for underdoped cuprates that it is permissible to linearize $\epsilon_{\mathbf{k}}$ and $\Delta_{\mathbf{k}}$ in the vicinity of the four nodes.[30] We implement this linearization by introducing a local coordinate system (k_1, k_2) centered at the nodal point with axes rotated 45° with respect to (k_x, k_y). Expanding to leading order, we have $\epsilon_{\mathbf{k}} \rightarrow v_F k_1$, $\Delta_{\mathbf{k}} \rightarrow v_\Delta k_2$ with v_F, v_Δ being the Fermi and gap velocities at the node, respectively. We thus obtain

$$\begin{aligned} \frac{1}{\lambda_{ab}^2} &= \frac{2e^2 Z_0^2 v_F^2 n}{d} \int_{E_{\mathbf{k}}<E_{\rm c}} \frac{dk_1 dk_2}{(2\pi)^2} \frac{v_\Delta^2 k_2^2}{E_{\mathbf{k}}^2} \\ &\times \left[\frac{1}{E_{\mathbf{k}}} \tanh \frac{1}{2}\beta E_{\mathbf{k}} - \frac{1}{2}\beta \mathrm{sech}^2 \frac{1}{2}\beta E_{\mathbf{k}} \right], \end{aligned} \tag{7}$$

where $E_{\mathbf{k}} = \sqrt{v_F^2 k_1^2 + v_\Delta^2 k_2^2}$ is the linearized "Dirac" spectrum of quasiparticles. It is now useful to rescale the integration variables as $v_F k_1 \to k_1$ and $v_\Delta k_2 \to k_2$ and pass to polar coordinates. The angular integral is trivial and we obtain (inserting $\hbar$ and k_B)

$$\frac{1}{\lambda_{ab}^2} = \frac{2e^2 Z_0^2 n v_{\rm F}}{\hbar^2 d\, v_\Delta} \int_0^{E_{\rm c}} \frac{dk}{4\pi} \Big[\tanh\frac{\beta k}{2} - \frac{\beta k}{2} \mathrm{sech}^2 \frac{\beta k}{2} \Big] , \quad (8a)$$

$$\simeq \frac{e^2 Z_0^2 n}{2\pi\hbar^2 d} \frac{v_{\rm F}}{v_\Delta} \left(E_{\rm c} - 4 k_B T \ln 2 \right) , \quad (8b)$$

where the second line applies in the regime $T \ll E_{\rm c}$.

It is clear that if we take $E_{\rm c} \propto x$, then this reproduces Eq. (1). To make a rough estimate of how $E_{\rm c}$ must vary with the T_c of an underdoped sample for this picture to apply, we simply assume that $T_{\rm c}$ may be determined by the T at which $\lambda_{ab}^{-2}(T)$ in Eq. (8b) equals 0. This criterion, which was also used by Lee and Wen,[14] gives $E_{\rm c} \simeq 2.8 k_{\rm B} T_{\rm c} = 0.24 T_{\rm c}$meV/K. Comparison with the experimental data shown in Fig. 2 illustrates that this overestimates T_c by about a factor of 2.3 due to the fact that the actual data deviates significantly from the straight line at higher temperatures. To account for this deviation, and for future reference, we revise our estimate to read

$$E_{\rm c} \simeq 6.4 k_{\rm B} T_{\rm c} = 0.55 T_{\rm c}\text{meV/K}. \quad (9)$$

This implies that even at optimal doping, $T_c \simeq 90$K, the energy scale $E_{\rm c}$ is of the order of maximum gap $\Delta_0 \simeq 45$meV. This validates our assumption that for underdoped YBCO the linearized approximation should lead to quantitatively correct results. Similarly one can estimate the doping dependence of $E_{\rm c}$ by comparing Eqs. (1) and (8b). For YBCO this yields

$$E_{\rm c} \simeq 2\pi a \frac{v_\Delta}{v_F} Z_0^{-2} x \approx [219.0\text{meV}] x, \quad (10)$$

where we have taken $Z_0^2 (v_F/v_\Delta) = 7$, a value relevant to this material.[11] In Sec. IV we shall see that a similar value of $E_{\rm c}$ also provides the best fit to c-axis penetration depth data.

There is an important caveat regarding the preceding analysis due to the fact that it relies on on the approximate formula Eq. (8b). Indeed, the exact formula Eq. (8a) does not possess a $T_{\rm c}$ in the sense of Eq. (8b): One can easily see that $\lambda_{ab}^{-2}(T) > 0$ for any T. This is because we have taken $\Delta_{\mathbf{k}}$ to be nonzero and temperature-independent as implied for underdoped cuprates by various experiments such as ARPES[31] or tunneling.[32] For non-zero pair potential within mean-field theory, the condensate is depleted only through thermal excitation of quasiparticles; this leaves a small fraction of electrons in the condensate at arbitrary temperatures. In other words within mean-field BCS theory the only way to kill the condensate is to drive $\Delta_{\mathbf{k}}$ to zero. In Fig. (2), we plot Eq. (8a) (solid line) and Eq. (8b) (dashed line) as a function of the normalized temperature $T/E_{\rm c}$. One can show that the solid line approaches zero only asymptotically as $1/T^3$. In any real system, once the superfluid stiffness becomes sufficiently small due to quasiparticle excitations, fluctuation effects (e.g., phase fluctuations[2]) will rapidly destroy the condensate. Thus, it is reasonable to assume that the relationship (9) holds approximately for real systems; i.e., it provides an estimate for how the physical $T_{\rm c}$ depends on the zero-temperature superfluid stiffness (parameterized by $E_{\rm c}$). In the next section, we compute the c-axis superfluid stiffness within a tunneling model and will find similar behavior.

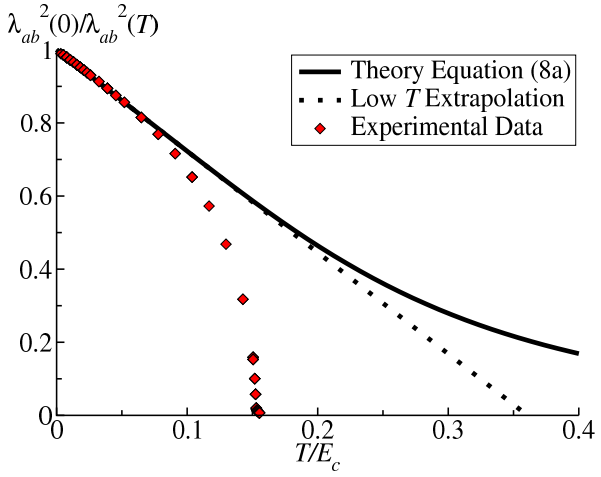

FIG. 2: Plot of normalized superfluid stiffness $(\lambda_{ab}(0)/\lambda_{ab}(T))^2$ with $\lambda_{ab}(T)$ given by Eq. (8a) (solid line) and Eq. (8b) (dashed line), respectively, as a function of the normalized temperature $T/E_{\rm c}$. Although they agree well at low temperatures, the deviation of Eq. (8b) from Eq. (8a) becomes significant at high temperatures. As noted in the text, Eq. (8a) never reaches zero, indicating that the quasiparticle-excitation mechanism of depleting the condensate can never fully destroy superconductivity if the pair potential remains nonzero. Diamonds represent the ab-plane data (YBCO 6.6) of Ref. [12] scaled in such a way that the low-T linear part agrees with the theoretical model.

Finally we may ask whether there is another form of $Z_{\mathbf{k}}$ that might agree with the experimental data. One possibility is that, for some reason, $Z_{\mathbf{k}}$ does not vanish outside the nodal patch but goes to a small value proportional to $\sqrt{x}$. This would clearly reproduce the observed ab-plane doping dependence.[33] We shall see below, however, that such a form would *not* produce the correct doping dependence for λ_c; the latter appears to dictate that $Z_{\mathbf{k}}$ vanishes outside the patch. Also, we have only considered situations when $Z_{\mathbf{k}}$ depends on the momentum through the energy $E_{\mathbf{k}}$. While this assumption appears very natural one can envision scenarios in which $Z_{\mathbf{k}}$ would depend on the individual components of $\mathbf{k}$.

III. c-AXIS PROPERTIES

In the present section, we apply the philosophy of Sec. II to the problem of the c-axis penetration depth, for which new data in the strongly underdoped regime has recently been obtained.[9,10]

A. Tunneling Hamiltonian

To model the electronic transport in the c-direction, we adopt the following tunneling Hamiltonian:

$$H_{\rm T} = \sum_{m,\sigma} \int d^2r (t_{\mathbf{r}} c^\dagger_{\mathbf{r},m+1,\sigma} c_{\mathbf{r},m,\sigma} + \text{h.c.}), \tag{11}$$

where $c_{\mathbf{r},m,\sigma}$ annihilates an electron at position $\mathbf{r}$ in layer m with spin projection σ. The matrix element $t_{\mathbf{r}}$ connects states in adjacent layers and is distinct from the quantity t in Sec. II. The total system Hamiltonian, then, consists of a sum of intralayer Hamiltonians given by Eq. (3) coupled by $H_{\rm T}$.

To compute the c-axis superfluid stiffness, we derive via the Kubo formula the response to an AC electric field $E(\mathbf{r},m,t) = E(\mathbf{r},m)e^{i\omega t}$ in the c-direction. To do this, we recall that such an electric field may be incorporated via the Peierls substitution

$$t_{\mathbf{r}} \to t_{\mathbf{r}} e^{i\frac{ed}{c}A(\mathbf{r},m)}, \tag{12}$$

where $A(\mathbf{r},m) = \frac{ic}{\omega}E(\mathbf{r},m)e^{i\omega t}$ and d is the interlayer spacing. The c-axis current density $j(\mathbf{r},m)$ is given by

$$\begin{aligned} j(\mathbf{r},m) = &-iet_{\rm r}(c^\dagger_{{\rm r},m+1,\sigma} c_{{\rm r},m,\sigma} - \text{h.c.}) \\ &+ \frac{e^2 d}{c} t_r A(\mathbf{r},m)(c^\dagger_{{\rm r},m+1,\sigma} c_{{\rm r},m,\sigma} + \text{h.c.}). \end{aligned} \tag{13}$$

The two terms in Eq. (13) have the familiar form of the paramagnetic and diamagnetic contributions to the current, respectively. We proceed to compute the associated contributions to the conductivity to leading order in perturbation theory in the matrix element $t_{\mathbf{r}}$. We shall furthermore assume that the in-plane Green functions are given by the usual d-wave BCS forms:

$$\langle T_\tau c_{-\mathbf{p},m,\downarrow}(\tau) c_{\mathbf{p},m',\uparrow}(0)\rangle = \delta_{m,m'} F(\mathbf{p},\tau), \tag{14a}$$

$$\langle T_\tau c_{\mathbf{p},m,\sigma}(\tau) c^\dagger_{\mathbf{p},m',\sigma}(0)\rangle = -\delta_{m,m'} G(\mathbf{p},\tau), \tag{14b}$$

with $G(\mathbf{p},\omega)$ and $F(\mathbf{p},\omega)$ given in Eq. (A12) and Eq. (A13), respectively.

Of principal importance is our choice for the form of the tunneling matrix element $t_{\mathbf{r}}$. Allowing for nontrivial $\mathbf{r}$-dependence is essential, as a spatially uniform $t_{\mathbf{r}}$ (so that in-plane momentum is conserved during the tunneling process) yields a T-linear correction to the penetration depth at low temperatures. This may be understood by noting that such purely coherent tunneling between layers simply yields a three-dimensional d-wave superconductor. As noted previously,[24,25] the absence of such linear behavior points towards incoherence in the c-axis tunneling. Before proceeding, we remark that another possibility to obtain non-linear-T dependence is the proposal of Xiang and Wheatley.[26] They find that by including a momentum dependence to the tunneling matrix element (arising from the structure of the copper and oxygen orbitals involved in tunneling), one finds a T^5 dependence in disagreement with the overall observed temperature dependence [Eq. (2)]. It is possible that such a T-dependent contribution is present but simply masked by the dominant T^2 behavior; however, we shall not include this possibility in the following.

Our strategy for finding a form for $t_{\mathbf{p}-\mathbf{k}}$ that gives the experimentally observed T-dependence is to assume that interplane disorder scatters the momentum states tunneling from layer to layer. We assume that the disorder-averaged matrix element $\overline{t_{\mathbf{k}}} = 0$. For the disorder-averaged product of tunneling matrix elements we choose

$$\overline{t^*_{\mathbf{k}} t_{\mathbf{k}+\mathbf{q}}} = (2\pi)^2 \delta(\mathbf{q}) \mathcal{T}_k^2, \tag{15a}$$

$$\mathcal{T}^2_{\mathbf{k}} = \frac{t_\perp^2}{\pi\Lambda^2} e^{-k^2/\Lambda^2}, \tag{15b}$$

with $t_\perp$ being an energy scale characterizing the strength of tunneling and Λ being an inverse length scale characterizing the degree of momentum non-conservation. We expect that the specific form of $\mathcal{T}^2_{\mathbf{k}}$ is unimportant as long as it includes the possibility of tunneling between different in-plane momentum states. Similar models that incorporate disorder in c-axis transport have been considered by the authors of Refs. [24,25] who also find T^2 behavior. In Ref. [25], it is assumed that $\mathcal{T}_{\mathbf{k}}$ depends only on the component of $\mathbf{k}$ *parallel* to the Fermi surface (implying complete non-conservation of the *perpendicular* component). Under these assumptions, the leading temperature dependence of $\lambda_c^{-2}(T)$ is quadratic, provided that the parallel component of $\mathbf{k}$ is conserved. It is however not easy to envision an interlayer scattering mechanism that would produce tunneling that is perfectly conserving for the momentum component parallel to the Fermi surface while totally non-conserving in the perpendicular direction. A much more natural assumption, embodied by our choice Eq. (15b), is to take $\mathcal{T}_{\mathbf{k}}$ to be *isotropic* in the ab-plane. In the next section, we turn to the evaluation of the c-axis penetration depth with this choice of tunneling matrix element. We will show that even isotropic tunneling produces a nearly T^2 dependence of $\delta\lambda_c(T)$ as a crossover behavior when the anisotropy of the Dirac spectrum near the node is taken into account. The same physics also produces the nearly x^2 doping dependence of $\lambda_c^{-2}(0)$, provided that we implement the charge renormalization factors as we did in the Sec. II

B. c-axis penetration depth

The calculation of the c-axis penetration depth within the tunneling Hamiltonian formalism parallels that presented in Appendix A for λ_{ab}. The details can be found in Ref. [25] and the result is given by

$$\frac{1}{\lambda_c^2} = 8e^2 d \sum_{\mathbf{k},\mathbf{p}} \mathcal{T}^2_{\mathbf{k}-\mathbf{p}} T \sum_{i\omega} F(\mathbf{k},\omega) F(\mathbf{p},\omega), \tag{16}$$

As noted in Ref. [25], this is equivalent to the standard result[34] for the critical Josephson current through a weak link. This is sensible, since the way in which supercurrent is passed in the c-direction for weakly coupled layers is via the Josephson effect.

We now augment Eq. (16) in the same manner as in Sec. II, by making the replacement

$$e^2 \sum_{\mathbf{k},\mathbf{p}} \rightarrow e^2 \sum_{\mathbf{k},\mathbf{p}} Z_{\mathbf{k}} Z_{\mathbf{p}}. \tag{17}$$

With the choice made for $Z_{\mathbf{k}}$ in Eq. (6) this again amounts to restricting the summations over $\mathbf{k}$ and $\mathbf{p}$ to within the vicinity of the nodes. Evaluating the sum over Matsubara frequencies, we obtain

$$\begin{aligned} \frac{1}{\lambda_c^2} \;=\; & 2e^2 d \sum_{\mathbf{k},\mathbf{p}} \mathcal{T}^2_{\mathbf{k}-\mathbf{p}} Z_{\mathbf{k}} Z_{\mathbf{p}} \frac{\Delta_{\mathbf{k}} \Delta_{\mathbf{p}}}{E_{\mathbf{k}} E_{\mathbf{p}}} \\ & \times \left[\frac{\tanh \frac{1}{2}\beta E_{\mathbf{k}} + \tanh \frac{1}{2}\beta E_{\mathbf{p}}}{E_{\mathbf{k}} + E_{\mathbf{p}}} \right. \\ & \left. - \frac{\tanh \frac{1}{2}\beta E_{\mathbf{k}} - \tanh \frac{1}{2}\beta E_{\mathbf{p}}}{E_{\mathbf{k}} - E_{\mathbf{p}}} \right]. \end{aligned} \tag{18}$$

This equation contains a four dimensional momentum integral and one needs to employ numerical methods to obtain the full T and E_c dependences of λ_c. We shall present such numerical results shortly. In order to elucidate the physics contained in this expression we first study the leading behavior analytically using scaling arguments in the limit of low T and low doping x [entering via $E_c \propto x$ as in Sec. (II)] when the physics is dominated by the nodal regions.

C. c-axis penetration depth: scaling analysis

Consider the low-T behavior of λ_c^2 for $T \ll E_c \ll \Delta_0$. We shall denote the T-dependent correction to the stiffness by $\delta\lambda_c(T) \equiv \lambda_c^{-2}(0) - \lambda_c^{-2}(T)$. An explicit expression for $\delta\lambda_c(T)$ may be obtained from Eq. (18) by replacing each tanh function by $1-\tanh$ (with the same argument). In the low-T limit, these functions restrict the momentum integrals to the vicinity of the nodes, so that we can take $Z_{\mathbf{k}} \simeq Z_0$ everywhere. Linearizing near the four nodes and rescaling to the natural momentum variables as in Eq. (8a) we find that the tunneling matrix element $\mathcal{T}^2_{\mathbf{k}}$ becomes *anisotropic*, as illustrated in Fig. 3. In these

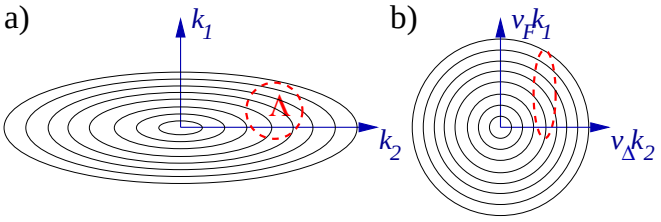

FIG. 3: Schematic plot of the constant energy contours in momentum space in the vicinity of a node. On the left, contours at energy $E_{\mathbf{k}}$ satisfy $E^2_{\mathbf{k}} = v_F^2 k_1^2 + v_\Delta^2 k_2^2$ (i.e., they are ellipses). The tunneling matrix element Eq. (15b) conserves momentum within a range Λ represented by the dashed circle. By rescaling the plot so that the axes are $v_F k_1$ and $v_\Delta k_2$, the constant energy contours are circles, but the circle representing the degree of momentum conservation has become distorted, indicating that the k_1 component of the quasiparticle momentum is effectively conserved to a lesser degree than k_2.

natural "nodal" variables the momentum component perpendicular to the Fermi surface ($v_F k_1$) is conserved to a lesser degree than the parallel component ($v_\Delta k_2$). This gives rise to three distinct scaling regimes depending on the magnitude of T with respect to the two natural scales of the problem, $v_F\Lambda$ and $v_\Delta\Lambda$. In what follows, we shall assume that $v_\Delta \ll v_F$, as is known to be the case for cuprates.[18]

(i) For $v_\Delta\Lambda \ll v_F\Lambda \ll T$ thermally excited quasiparticles tunnel between the layers essentially as if momentum were conserved, i.e., Λ is a small scale in this regime. In this limit we may approximate $\mathcal{T}^2_{\mathbf{k}-\mathbf{p}}$ by a delta function and Eq. (18) becomes the same as the result Eq. (4) for λ_{ab}, implying *linear* temperature dependence, $\delta\lambda_c(T) \sim T$.

(ii) For $v_\Delta\Lambda \ll T \ll v_F\Lambda$ the form of $\mathcal{T}^2_{\mathbf{k}-\mathbf{p}}$ suggests that the dominant tunneling is characterized by $v_\Delta k_2$ being essentially conserved but $v_F k_1$ being essentially unrestricted. This is exactly the situation envisioned in Ref. [25], leading to the T^2 behavior, but in our case it emerges as a crossover phenomenon.

(iii) For $T \ll v_\Delta\Lambda \ll v_F\Lambda$, extending this simple argument (so that neither component is conserved) yields a vanishing result for $\delta\lambda_c(T)$ due to the sign-change in the d-wave pair potential. Using a more careful Sommerfeld-like expansion detailed in Appendix B, we find that $\delta\lambda_c(T) \propto T^3$ in this regime.

Summarizing, we have

$$\delta\lambda_c(T) \sim \begin{cases} T^3 & \text{for } T \ll v_\Delta\Lambda \ll v_F\Lambda; \\ T^2 & \text{for } v_\Delta\Lambda \ll T \ll v_F\Lambda; \\ T & \text{for } v_\Delta\Lambda \ll v_F\Lambda \ll T. \end{cases} \tag{19}$$

The c-axis penetration depth data of Ref. [9,10] exhibit power-law behavior consistent with T^3 crossing over to T^2. The first two regimes of Eq. (19) indicate that, by a suitable choice of the parameter Λ, it may be possible to

fit this data with the present model. Before attempting such a fit, we turn to the E_c dependence of $\lambda_c^{-2}(0)$.

Next, we carry out a similar analysis for $\lambda_c^{-2}(0)$, which has the explicit form of Eq. (18) but with each tanh function replaced by unity. In analyzing $\delta\lambda_c(T)$, we made use of the interplay between the way in which integrals were cut off by T and the way momenta were effectively conserved by $\mathcal{T}^2_{\mathbf{k}-\mathbf{p}}$. For $\lambda_c^{-2}(0)$, the momentum integrals are cut off by E_c instead of T (via the factor $Z_{\mathbf{k}}Z_{\mathbf{p}}$), but otherwise the previous analysis remains largely valid. In particular, the intermediate ($v_\Delta\Lambda \ll E_c \ll v_F\Lambda$) and high ($v_\Delta\Lambda \ll v_F\Lambda \ll E_c$) E_c regimes are analogous to their counterparts in Eq. (19). At low E_c, the naive analysis fails (as it did for $\delta\lambda_c(T)$ at low T); a more careful analysis (described in Appendix B) shows that $\lambda_c^{-2}(0) \propto E_c^5$ for $E_c \to 0$. We thus have

$$\lambda_c^{-2}(0) \sim \begin{cases} E_c^5 & \text{for } E_c \ll v_\Delta\Lambda \ll v_F\Lambda; \\ E_c^2 & \text{for } v_\Delta\Lambda \ll E_c \ll v_F\Lambda; \\ E_c & \text{for } v_\Delta\Lambda \ll v_F\Lambda \ll E_c. \end{cases} \quad (20)$$

Our results (19) and (20) indicate that the incoherent tunneling model with effective charge renormalization (6) qualitatively reproduces the trends in the c-axis penetration depth summarized in Eq. (2). The near-quadratic behavior in both temperature and doping observed in experiment[9,10] emerges in our model as a crossover phenomenon involving the energy scales $v_\Delta\Lambda \ll v_F\Lambda$. We shall see below that the full numerical integration of Eq. (18) indeed reproduces the scaling behavior indicated in Eqs. (19), (20) and furthermore gives excellent *quantitative* agreement with the experimental data.

From our analysis above it should also be clear that if $Z_{\mathbf{k}}$ fell to a small value proportional to $\sqrt{x}$ outside the nodal patch (instead of vanishing there) then $\lambda_c^{-2}(0)$ would pick up a contribution *linear* in x in all the regimes described in Eq. (20), in disagreement with the data.

D. c-axis penetration depth: numerical evaluation

To facilitate numerical evaluation it is useful to rewrite Eq. (18) by converting the sums to integrations in the usual way and switching to relative and center-of-mass variables $\mathbf{q} = (\mathbf{k}-\mathbf{p})/2$ and $\mathbf{Q} = (\mathbf{k}+\mathbf{p})/2$. We have

$$\frac{1}{\lambda_c^2} = \frac{16e^2d}{(v_F v_\Delta)^2}\int\frac{d^2Q}{(2\pi\hbar)^2}\int\frac{d^2q}{(2\pi\hbar)^2} Z_{\mathbf{Q}+\mathbf{q}}Z_{\mathbf{Q}-\mathbf{q}} \quad (21)$$
$$\times\mathcal{T}^2_{2\tilde{\mathbf{q}}}\frac{q_2^2-Q_2^2}{|\mathbf{Q}+\mathbf{q}||\mathbf{Q}-\mathbf{q}|}\frac{1}{\mathbf{q}\cdot\mathbf{Q}}$$
$$\times\left[|\mathbf{Q}-\mathbf{q}|\tanh\frac{|\mathbf{Q}+\mathbf{q}|}{2T} - |\mathbf{Q}+\mathbf{q}|\tanh\frac{|\mathbf{Q}-\mathbf{q}|}{2T}\right],$$

where we have also linearized in the vicinity of the nodes and rescaled the momenta $v_F Q_1 \to Q_1$ and $v_\Delta Q_2 \to Q_2$ and similarly for $\mathbf{q}$. Such a rescaling effectively makes the argument of the matrix element factor anisotropic: In Eq. (21) its argument is $\tilde{\mathbf{q}} \equiv (q_1/v_F, q_2/v_\Delta)$.

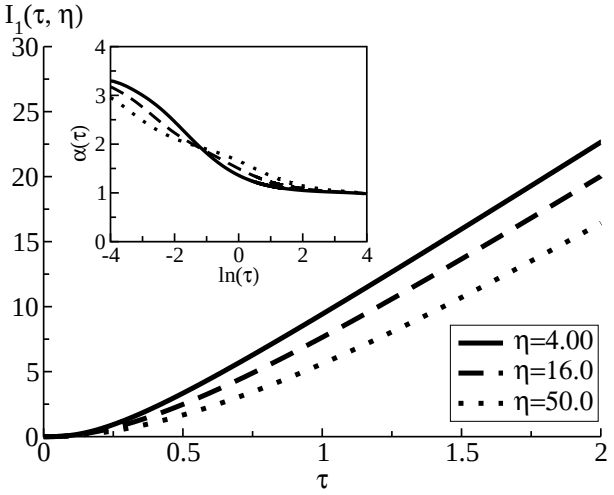

FIG. 4: Plot of $I_1(\tau,\eta)$ for $\eta = 4, 16, 50$. To emphasize the crossover behavior in the power-law of $I_1(\tau,\eta)$, the inset plots the associated logarithmic derivative $\alpha(\tau) = d\ln I_1/d\ln\tau$.

Before proceeding, we re-emphasize that incoherence in the tunneling matrix element is essential for obtaining the correct temperature dependence of $\lambda_c(T)$ (and, with our choice for $Z_{\mathbf{k}}$, the correct doping dependence of $\lambda_c(T)$). For the case $\Lambda \to 0$, in which the spatially modulated tunneling matrix element becomes uniform on average, Eq. (21) yields a T-linear finite temperature correction $\lambda_c^{-2}(0) - \lambda_c^{-2}(T)$. Thus, incoherence in the tunneling matrix element is crucial in what follows.

It is convenient to express all quantities as dimensionful prefactors multiplying dimensionless functions of dimensionless parameters. We express $\delta\lambda_c(T)$ in this manner as

$$\delta\lambda_c(T) = \frac{16e^2\Lambda d}{\pi\sqrt{v_F v_\Delta}}\frac{Z_0^2 t_\perp^2}{h^4} I_1\left(\frac{T}{\sqrt{v_F v_\Delta}\Lambda},\eta\right), \quad (22a)$$

$$I_1(\tau,\eta) \equiv 4\tau^3\int d^2q\, e^{-4\tau^2(q_1^2/\eta - q_2^2\eta)}\Omega(\mathbf{q}), \quad (22b)$$

$$\Omega(\mathbf{q}) \equiv \frac{1}{4}\int d^2Q\frac{q_2^2-Q_2^2}{|\mathbf{Q}+\mathbf{q}||\mathbf{Q}-\mathbf{q}|}\frac{1}{\mathbf{q}\cdot\mathbf{Q}}$$
$$\times\left[|\mathbf{Q}-\mathbf{q}|(1-\tanh\frac{|\mathbf{Q}+\mathbf{q}|}{2}) - \right.$$
$$\left. -|\mathbf{Q}+\mathbf{q}|(1-\tanh\frac{|\mathbf{Q}-\mathbf{q}|}{2})\right]. \quad (22c)$$

For simplicity in the above integrals we have set $Z_{\mathbf{k}}$=Z_0, an approximation valid as long as $T \ll E_c$. The integrals remain convergent due to the thermal Fermi factors.

In the main part of Fig. 4 we display $I_1(\tau,\eta)$ for $\eta = 4, 16, 50$; other values of η display similar behavior. To focus on the power-law behavior of $I(\tau,\eta)$, in the inset of Fig. 4 we plot the logarithmic derivative $\alpha(\tau) = d\ln I_1/d\ln\tau$ as a function of $\ln\tau$, again for $\eta = 4, 16, 50$. The virtue of such a plot is that constant behavior of the logarithmic derivative at a particu-

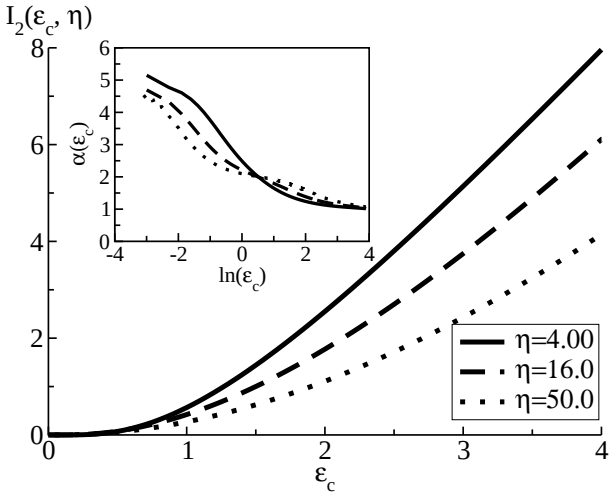

FIG. 5: Plot of $I_2(\varepsilon_c,\eta)$ for $\eta = 4, 16, 50$. To emphasize the crossover behavior in the power-law of $I_2(\varepsilon_c,\eta)$, the inset plots the associated logarithmic derivative $\alpha(\varepsilon_c) = d\ln I_2/d\ln\varepsilon_c$.

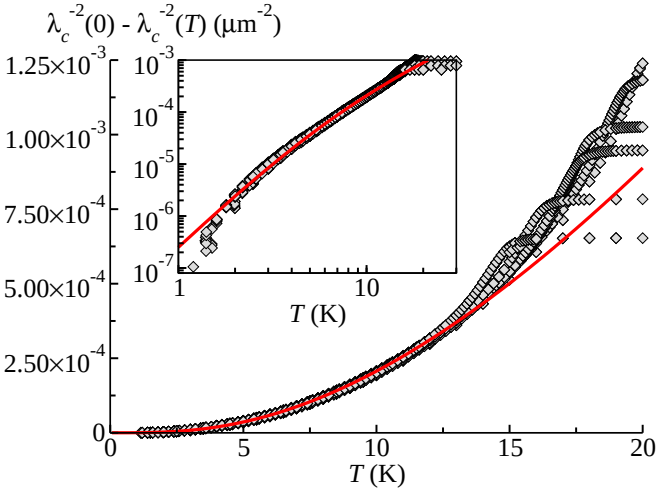

FIG. 6: Plot of fits to experimental data of Ref. [9, 10]. The diamonds are $\lambda_c^{-2}(0) - \lambda_c^{-2}(T)$ for various dopings having experimental T_c values (top to bottom) 20.2, 19.5, 18.2, 17.8, 16.4, 15.1K. The solid curve is our best fit using the parameters $\hbar\Lambda^{-1} = 120$Å and $t_\perp = 26$meV. The inset is the same plot on a logarithmic scale, showing the changing power law of the experimental data and of our theoretical curve.

lar value reflects power-law behavior of $I(\tau,\eta)$ with that value as the exponent. By examining this plot, there is clear evidence for τ-linear behavior for $\tau \gg \sqrt{\eta}$ (in fact, the exponent approaches unity for much lower values of τ) and τ^3 behavior for $\tau \ll 1/\sqrt{\eta}$. At intermediate τ the exponent is close to 2 although the expected plateau starts developing only for large anisotropy η. We may thus conclude that $\delta\lambda_c(T)$ indeed exhibits behavior expected from the scaling analysis presented above.

We now analyze the doping dependence. It is convenient to express $\lambda_c^{-2}(0)$ in a form reminiscent of Eq. (22a); i.e., as a product of a dimensionful prefactor multiplying a dimensionless function of suitably chosen dimensionless quantities. We thus have

$$\frac{1}{\lambda_c^2(0)} = \frac{16e^2\Lambda d}{\pi\sqrt{v_F v_\Delta}}\frac{Z_0^2 t_\perp^2}{h^4} I_2\Big(\frac{E_c}{\sqrt{v_F v_\Delta}\Lambda},\eta\Big), \quad (23a)$$

$$I_2(\varepsilon_c,\eta) = \varepsilon_c^3 \int_1 d^2k \int_1 d^2p\, \frac{k_2 p_2}{kp}\frac{1}{k+p} \times e^{-\varepsilon_c^2[(k_1-p_1)^2/\eta-(k_2-p_2)^2\eta]}, \quad (23b)$$

where the subscript 1 on the integrations in Eq. (23b) indicate that the integration range is the unit disk, corresponding to the discontinuous jump in our choice for $Z_{\mathbf{k}}$. In practice, for numerical convenience we shall replace this hard cutoff with a Gaussian soft cutoff when performing numerical integrals. This corresponds to the choice $Z_{\mathbf{k}} = Z_0\exp(-E_{\mathbf{k}}^2/E_c^2)$ which leads to the same qualitative ab-plane behavior as discussed in Sec. II.

To ascertain whether the three regimes indicated in Eq. (20) are indeed realized, in the main part of Fig. 5 we display a numerical plot of $I_2(\varepsilon_c,\eta)$ for $\eta = 4, 16, 50$. The inset of Fig. 5 we plot the logarithmic derivative of this quantity. For large ε_c, $I_2(\varepsilon_c,\eta)$ clearly exhibits linear behavior. For intermediate ε_c, there is clearly a regime of quadratic behavior that is more pronounced for the cases $\eta = 16$ and $\eta = 50$ and the exponent is seen to approach 5 for low ε_c. The essential feature of $I_2(\varepsilon_c,\eta)$ is that it exhibits power-law behavior with an exponent near 2 for a considerable range of ε_c. The hope is that this quadratic dependence can, with a suitable choice of parameters, fit the known quadratic doping dependence of the c-axis penetration depth Eq. (2). In the next section, we perform a detailed fit to c-axis data.[9,10]

IV. c-AXIS PENETRATION DEPTH: DATA FITS

In the present section, we attempt to fit the c-axis penetration depth data of Ref. [9,10] using the theoretical formulas obtained in the preceding section. Thus, we assume that the experimental $\lambda_c^{-2}(T) \approx \lambda_c^{-2}(0) - \delta\lambda_c(T)$ with $\lambda_c^{-2}(0)$ and $\delta\lambda_c(T)$ being given by Eq. (23a) and Eq. (22a), respectively. Within this approximation to Eq. (21), $\delta\lambda_c(T)$ does not depend on E_c, in agreement with the experimental observation that the finite-T correction is universal (i.e. doping-independent) at low T. Thus, we begin by first fitting $\delta\lambda_c(T)$ to the experimental finite-T correction $\lambda_c^{-2}(0) - \lambda_c^{-2}(T)$.

The relevant fitting parameters are as follows: The parameters $t_\perp$ and Λ characterize the way in which tunneling occurs in the c-axis direction; since the measurements of Ref. [9,10] were done on one crystal, we shall take these to be *global* fitting parameters. The parameter Z_0 may be taken to be unity, as it only enters in Eq. (23a) and

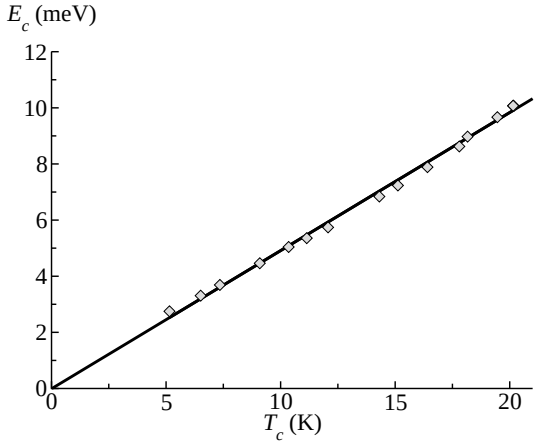

FIG. 7: Plot of extracted values of the charge-renormalization parameter E_c (diamonds) as a function of the experimental T_c, showing a linear behavior as a function of doping level. The solid curve is a linear fit to these values, and has the form $E_c = 0.49T_c/\mathrm{K} + 0.01(\mathrm{meV})$.

Eq. (22a) in the product $Z_0 t_\perp$. We take $v_\mathrm{F} = 1.8$ eV Å[11] and $d = 5.85$Å, although it is not known if v_F changes for strongly underdoped samples. As discussed above, the way in which the power-law behavior of Eq. (22a) changes as quasiparticles are excited from the condensate depends on the magnitude of the anisotropy ratio $\eta = v_\mathrm{F}/v_\Delta$; however, in practice we have not found the quality of the fits to be strongly dependent on this value. Thus, although the best fits (i.e. those minimizing the variance) were found with the value $\eta = 6.8$, one cannot claim to extract a value for η using this technique. The converse of this is that although it is expected that η will vary somewhat for such underdoped samples (in a way that is not understood at present), the weak dependence of the quality of our fits on η validates our neglecting this doping dependence.

In Fig. 6 we show our best fits to the low-temperature values of $\lambda_c^{-2}(0) - \lambda_c^{-2}(T)$ in the experiments of Ref. [9, 10]. The diamonds represent data curves for a particular doping value. Each doping value is characterized by a particular T_c which we take to be proportional to x. For clarity we have only displayed the highest doping values (i.e., $T_\mathrm{c} = 20.2, 19.5, 18.2, 17.8, 16.4, 15.1$K); the fits are equally good for lower doping values. The solid line is our best fit with the parameters $\hbar/\Lambda = 120$Å and $t_\perp = 26$meV. The fits work well at low T (despite the fact that the data is *not* a simple power law) but begins to deviate at high temperatures. (The roughly horizontal behavior occurs above T_c). We ascribe this discrepancy to fluctuation effects near T_c in a given sample, as well as the fact that we have neglected the effect of $Z_\mathbf{k}$ on the finite temperature correction $\delta\lambda_c(T)$ in Eq. (22a). This restricts the validity of our calculations to low temperature. As we saw in Sec. II for λ_{ab}, the deviations due to this effect are expected to become more pronounced at higher temperatures (see Fig. 2).

Having fit the temperature-dependent correction, the *only* remaining parameters are the values of E_c corresponding to a particular doping. We extract these using Eq. (23a) for $\lambda_c^{-2}(0)$. In Sec. II we noted that to account for the *ab*-plane phenomenology, we must have $E_\mathrm{c} \propto x$ (and therefore $E_\mathrm{c} \propto T_\mathrm{c}$). To verify that this indeed holds, in Fig. 7 we plot (diamonds) the extracted best-fit values of E_c for a given experimental T_c from the Hosseini *et al.* results. The solid curve is a linear fit to these values, with the form $E_\mathrm{c} = 0.49T_\mathrm{c}/\mathrm{K} + 0.01(\mathrm{meV})$. This agrees very well with the rough estimate of Sec. II where we found $E_\mathrm{c} = 0.55T_c$ meV/K from the *ab* plane data. This linear "Uemura"[6] relation is an important constraint on this theory and depicts the destruction of the Fermi surface as the Mott insulating phase is approached at low doping values.

Finally, to illustrate the overall agreement of our model with the data, in Fig. 8 we plot the data of Hosseini *et al.*[9,10] for several representative doping values along with our curve fits. The agreement is strikingly good at low temperatures for all doping levels. We emphasize that all data sets are fit with a single set of parameters (listed in Fig. 8); the only parameter that varies is the cutoff energy according to $E_c = 0.49T_c$meV/K with T_c being the actual measured critical temperature.

V. CONCLUDING REMARKS

In an effort to understand *ab*-plane and *c*-axis superfluid stiffness in underdoped cuprates we have constructed a model incorporating incoherent tunneling between the CuO_2 planes along with a strongly anisotropic charge renormalization factor $Z_\mathbf{k}$. Incoherent tunneling provides a mechanism for obtaining a non-linear temperature dependence of λ_c^{-2} while the charge renormalization factor is introduced as means to model the fundamental departure from the BCS theory in the underdoped regime where only doped holes contribute to the superfluid.

At this stage our choice for $Z_\mathbf{k}$ is purely phenomenological and expands upon the suggestions of Refs. [11] and [27]. It is motivated by the observation[14] that although the *ab*-plane and *c*-axis penetration depths are strongly doping dependent, the temperature-dependent corrections to these doping-dependent values are nearly doping-independent. At the coarsest level, this implies that quasiparticle effective charge $Z_\mathbf{k} \simeq 1$ for states near the nodes of the *d*-wave order parameter but is strongly reduced away from the nodes in a doping-dependent fashion. This doping dependence is governed by a cutoff energy $E_\mathrm{c} \sim x$. By incorporating these two features into a model of the *ab*-plane and *c*-axis penetration depths, we were able to explain the low-temperature data[9,10] with a striking accuracy using a single set of input parameters and values of E_c which vary remarkably linearly with doping level, as expected on the basis of the *ab*-plane phenomenology.

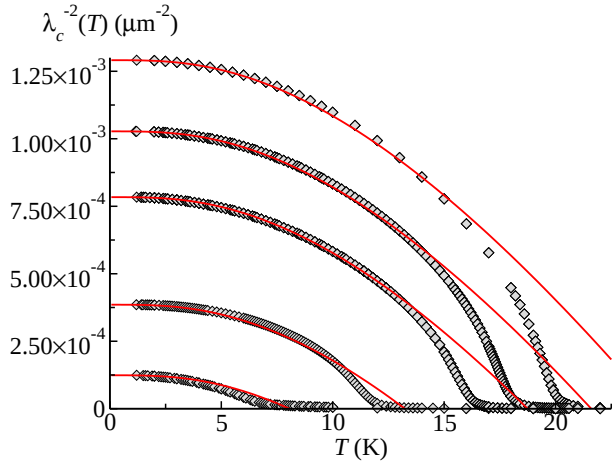

FIG. 8: Fit to data of Ref. [9,10] (diamonds) using parameters extracted in text. The T_c values are T_c = 20.2, 18.2, 16.4, 12.1, 7.4K, (top to bottom) representing decreasing effective doping. The parameters used are $\hbar\Lambda^{-1}$ = 120Å $t_\perp$ = 26meV, $\eta = v_F/v_\Delta$ = 6.8 and E_c = $0.49T_c$meV/K.

Taken together the above results lead to the notion of a "nodal protectorate" in which coherent BCS quasiparticles persist even as the system approaches the Mott-Hubbard insulating state near the half filling. This nodal protectorate is schematically depicted in Fig. 1 which in addition illustrates how the protected regions shrink to essentially nothing as $x \to 0$. The existence of this nodal protectorate is in addition supported by heat conduction[18], scanning tunneling spectroscopy[36] and photoemission experiments[37].

The existence of the nodal protectorate imposes a number of stringent constraints on any microscopic theory describing the the underdoped regime. In particular any such theory must explain what protects the low-energy nodal excitations from the strong interactions that otherwise drive the electrons in the remainder of the Brillouin zone inert to applied electromagnetic fields. In addition one would like to understand what is the significance of the energy scale $E_c \sim x$ implied by our results. It is well known that RVB-type theories[19] naturally explain the x-linear dependence of $\rho_s^{ab}(0)$ but predict a coefficient of the T-linear term to go as x^2, in strong disagreement with the experimental data. It has been claimed that the SU(2) version of the theory rectifies this problem[14] but the physics of this is somewhat opaque and the status of this result remains unclear.[38] In addition it is not obvious that one would obtain the required c-axis behavior from this model. Approaches which seek to describe the Mott physics via Gutzwiller projection techniques applied to the BCS wavefunction[20,21] also obtain the correct $\rho_s^{ab}(0) \sim x$ behavior. It is more difficult to address the finite-T properties within these models and the behavior of $\delta\lambda_{ab}(T)$ is not known at present. However, these being real space techniques, it is not easy to envision a mechanism that would protect the nodal regions from the strong correlations imposed by the projection and one would naively expect that the result will suffer from the same problem as the RVB theories.

It has been argued that the x and T dependence of ρ_s^{ab} can be explained within the Fermi liquid theory for superconductors with anisotropic Fermi surface[39,40] assuming a particular form of the interaction $f_{\mathbf{kk'}}^{\sigma\sigma'}$. We have checked that a most straightforward extension of this interaction does not reproduce the c-axis phenomenology; one would have to impose another set of constraints for the interlayer interactions to get the observed behavior which makes this route somewhat implausible in our view. One could imagine a competing order[41,42] in the particle-hole channel gapping out the Fermi surface away from the nodes, thus reducing the number of electrons participating in the superfluid in a manner consistent with the observed phenomenology.[43,44] The advantage of this scenario is that nodal quasiparticles would automatically remain protected and the c-axis phenomenology would presumably also follow. On the other hand such competing orders necessarily break various space-time symmetries of the underlying system and such symmetry breaking should be easily observable if the competing order was strong enough to modify the superfluid response in accord with experiment. On balance we feel that the available evidence does not support this scenario.[29]

In the phase fluctuation scenarios[2,4,5,6] the low superfluid density $\rho_s(0) \sim x$ enters as a phenomenological input. An appealing feature of these models is that in the superconducting state the phase fluctuations are gapped (with the gap of the order of $\rho_s \sim E_c$) and thus do not affect the low energy nodal quasiparticles which remain sharp even as $x \to 0$. On the other hand the phase fluctuation models require some microscopic theory to describe the Mott physics that is ultimately responsible for the assumed low superfluid density.

It would thus appear that none of the microscopic theories that exist at the present time satisfies all of the constraints implied by the phenomenological model advocated in this paper. We may conclude that the physics of a d-wave superconductor on the brink of becoming a Mott-Hubbard insulator remains an intellectual challenge awaiting future solution.

Acknowledgments — We wish to thank D.A. Bonn, D.M. Broun, W.N. Hardy, A. Hosseini and R. Liang for numerous valuable discussions and for providing their experimental data. In addition we are indebted to P.A. Lee, A.J. Millis, C. Nayak, X.-G. Wen and Z. Tesanovic for discussions and correspondence. We thank I. Olabarrieta for assistance with numerical computations which were performed in part on the vn.physics.ubc.ca cluster, funded by the Canadian Foundation for Innovation (CFI) and the BC Knowledge Development Fund. Part of this work was carried out at the Aspen Center for Physics. This work was supported by NSERC, CIAR and the A.P. Sloan Foundation.

APPENDIX A: CALCULATION OF λ_{ab}

In the present section, we compute the in-plane penetration depth for a BCS d-wave superconductor described by the Hamiltonian H in Eq. (3) with $H_{\rm int}=0$ for now. This is related to the imaginary part of the in-plane conductivity $\sigma_2(\omega)$ via[35]

$$\frac{1}{\lambda_{ab}^2}=\lim_{\omega\to 0}\omega\sigma_2(\omega). \tag{A1}$$

The first step is to identify how the system couples to an applied electric field E_x in the x direction. For the case of H having only nearest-neighbor hopping, the electromagnetic current operator has the form

$$j_x(\mathbf{r})=iea\sum_\sigma(tc^\dagger_{\mathbf{r},\sigma}c_{\mathbf{r}+a\hat{x},\sigma}-\text{h.c.}), \tag{A2}$$

with a being the lattice spacing. The coupling to the electromagnetic vector potential A_x (related to E_x via $A_x=-\frac{ic}{\omega}E_x e^{-i\omega t}$) enters by making the Peierls replacement $t\to t\exp(ieaA_x/c)$ in Eq. (A2). Expanding to to leading order in A, we have $j_x=j_x^{\rm p}+j_x^{\rm d}$ with the paramagnetic and diamagnetic currents being given, respectively, by

$$j_x^{\rm p} = ieat\sum_\sigma(c^\dagger_{\mathbf{r},\sigma}c_{\mathbf{r}+a\hat{x},\sigma}-\text{h.c.}), \tag{A3}$$

$$j_x^{\rm d} = -\frac{e^2a^2t}{c}\sum_\sigma(c^\dagger_{\mathbf{r},\sigma}c_{\mathbf{r}+a\hat{x},\sigma}+\text{h.c.})A_x. \tag{A4}$$

Our task is to find the conductivity $\sigma_{\rm L}(\omega)$ for a single layer, which is defined by $\langle j_x(q,\omega)\rangle=\sigma(q,\omega)E_x(q,\omega)$. The conductivity of the layered cuprate system will then be $\sigma(\omega)=\frac{n}{d}\sigma_{\rm L}(\omega)$ with n being the number of CuO_2 planes per layer and d being the interlayer spacing. The angle brackets represent the equilibrium average with respect to H, and henceforth we shall be concerned only with the $\mathbf{q}\to\mathbf{0}$ limit. In this limit, the Fourier transformed paramagnetic and diamagnetic current operators may be written as

$$j_x^{\rm p} = e\sum_{\mathbf{k},\sigma}\frac{\partial\epsilon_{\mathbf{k}}}{\partial k_x}c^\dagger_{\mathbf{k},\sigma}c_{\mathbf{k},\sigma}, \tag{A5}$$

$$j_x^{\rm d} = \frac{ie^2}{\omega}\sum_{\mathbf{k},\sigma}\frac{\partial^2\epsilon_{\mathbf{k}}}{\partial k_x^2}c^\dagger_{\mathbf{k},\sigma}c_{\mathbf{k},\sigma}E_x, \tag{A6}$$

where we have displayed the expression for general $\epsilon_{\mathbf{k}}$ (and will continue to do so henceforth). The frequency dependent conductivity per layer is

$$\sigma_{\rm L}(\mathbf{0},\omega)=\frac{i}{\omega}[D+\Pi^{\rm R}(\omega)], \tag{A7}$$

where D and Π represent the diamagnetic and paramagnetic parts of the response. As usual, the diamagnetic current is already linear in the electric field so that the associated contribution to the conductivity can be directly read off by taking the expectation value of Eq. (A6),

$$D = e^2\sum_{\mathbf{k},\sigma}\frac{\partial^2\epsilon_{\mathbf{k}}}{\partial k_x^2}\langle c^\dagger_{\mathbf{k},\sigma}c_{\mathbf{k},\sigma}\rangle, \tag{A8}$$

$$= 2e^2T\sum_{i\omega}\sum_{\mathbf{k}}\frac{\partial^2\epsilon_{\mathbf{k}}}{\partial k_x^2}G(\mathbf{k},\omega). \tag{A9}$$

For the paramagnetic current, the usual leading-order perturbation theory result[34] naturally leads to considering the current-current correlator

$$\Pi(\nu) = -\int_0^\beta d\tau e^{-i\nu\tau}\langle T_\tau j^{\rm p}(\tau)j^{\rm p}(0)\rangle, \tag{A10}$$

$$= 2e^2T\sum_{i\omega}\sum_{\mathbf{k}}\left(\frac{\partial\epsilon_{\mathbf{k}}}{\partial k_x}\right)^2[G(\mathbf{k},\omega)G(\mathbf{k},\omega-\nu) +F(\mathbf{k},\omega)F(\mathbf{k},\omega-\nu)], \tag{A11}$$

where the in-plane Matsubara Green functions $G(\mathbf{k},\omega)$ and $F(\mathbf{k},\omega)$ are given by the usual expressions

$$G(\mathbf{k},\omega) = \frac{i\omega+\epsilon_{\mathbf{k}}}{(i\omega)^2-E_{\mathbf{k}}^2}, \tag{A12}$$

$$F(\mathbf{k},\omega) = -\frac{\Delta_{\mathbf{k}}}{(i\omega)^2-E_{\mathbf{k}}^2}, \tag{A13}$$

and $E_{\mathbf{k}}\equiv\sqrt{\epsilon_{\mathbf{k}}^2+\Delta_{\mathbf{k}}^2}$. Performing the required Matsubara sums and combining the preceding expressions with Eq. (A1), we find the penetration depth

$$\frac{1}{\lambda_{ab}^2}=\frac{e^2n}{d}\sum_{\mathbf{k}}\frac{\partial^2\epsilon_{\mathbf{k}}}{\partial k_x^2}\left(1-\frac{\epsilon_{\mathbf{k}}}{E_{\mathbf{k}}}\tanh\frac{1}{2}\beta E_{\mathbf{k}}\right) -\frac{e^2n}{2d}\beta\sum_{\mathbf{k}}\left(\frac{\partial\epsilon_{\mathbf{k}}}{\partial k_x}\right)^2\text{sech}^2\frac{1}{2}\beta E_{\mathbf{k}}, \tag{A14}$$

with $\beta=1/T$ the inverse temperature. This last expression agrees with the results for λ_{ab} in the lattice model of a d-wave superconductor obtained by other authors.[28,29]

As written, the diamagnetic term in Eq. (A14) has contributions from the entire Brillouin zone while the paramagnetic term is dominated by the nodal regions ($E_{\mathbf{k}}\to 0$). For our purposes it will be convenient to recast the former into a form where it is also dominated by the nodal regions. This can be accomplished by integrating by parts in the first term of Eq. (A14). We obtain

$$\frac{1}{\lambda_{ab}^2} = \frac{e^2n}{d}\sum_{\mathbf{k}}\left[\left(\frac{\partial\epsilon_{\mathbf{k}}}{\partial k_x}\right)^2\frac{\Delta_{\mathbf{k}}^2}{E_{\mathbf{k}}^2}-\frac{\partial\epsilon_{\mathbf{k}}}{\partial k_x}\frac{\partial\Delta_{\mathbf{k}}}{\partial k_x}\frac{\Delta_{\mathbf{k}}\epsilon_{\mathbf{k}}}{E_{\mathbf{k}}^2}\right] \times\left[\frac{1}{E_{\mathbf{k}}}-\frac{\partial}{\partial E_{\mathbf{k}}}\right]\tanh\frac{1}{2}\beta E_{\mathbf{k}}. \tag{A15}$$

This expression is mathematically equivalent to Eq. (A14) and gives λ_{ab} as a k-space sum dominated

by the nodal regions. In addition, Eq. (A15) has the desirable property of explicitly yielding zero superfluid stiffness in the normal limit, $\Delta_{\mathbf{k}} = 0$. Finally we notice that the second term in the first line of Eq. (A15) is generally small for a d-wave gap. In particular it vanishes identically in the nodal approximation that we employ in Sec. II. Thus, we shall ignore this term.

APPENDIX B: ASYMPTOTIC BEHAVIOR OF $\delta\lambda_c(T)$ AND $\lambda_c^{-2}(0)$

In the present section we sketch the derivation of the low T behavior of $\delta\lambda_c(T)$ and the low $E_{\rm c}$ behavior of $\lambda_c^{-2}(0)$, i.e., the first lines of Eq. (19) and Eq. (20), respectively. For $Z_{\mathbf{k}}$ we use the smooth form $Z_{\mathbf{k}} = Z_0 \exp(-E_{\mathbf{k}}^2/E_c^2)$ introduced in Sec. III D. We will omit unimportant prefactors and, for simplicity, set $v_{\rm F} = v_\Delta = 1$. It will be clear from the derivation that relaxing this last assumption will not change the results. We begin with $\delta\lambda_c(T)$, which is given by

$$\delta\lambda_c(T) \;\propto\; \int \frac{d^2p}{(2\pi\hbar)^2}\frac{d^2k}{(2\pi\hbar)^2} \mathrm{e}^{-(\mathbf{k}-\mathbf{p})^2/\Lambda^2} \frac{k_2 p_2}{kp} \times \frac{p(1-\tanh(k/2T))}{p^2-k^2}. \tag{B1}$$

Henceforth, the polar coordinate expressions of $\mathbf{k}$ and $\mathbf{p}$ are (k,θ) and (p,ϕ), respectively. Our strategy is to utilize the following Sommerfeld expansion:

$$\begin{aligned}\int_0^\infty dk f(k)(1-\tanh k/2T) \qquad\qquad (B2)\\ \approx \int_0^\infty dk[f(0)+kf'(0)+\cdots](1-\tanh k/2T),\end{aligned}$$

which relies on the sharpness of the function $1-\tanh k/2T$ near $k=0$ for $T\to 0$ and is valid provided that the function $f(k)$ is sufficiently smooth near $k=0$. In the present case, the function f is given by (again, up to numerical prefactors)

$$f(k) = \int dp\, d\phi\, d\theta \frac{kp^2 \sin\theta \sin\phi}{p^2-k^2} \mathrm{e}^{-(\mathbf{k}-\mathbf{p})^2/\Lambda^2}. \tag{B3}$$

The first thing to note is that, due to the factor of k in Eq. (B3) (in turn arising from the k in the measure of Eq. (B1)), $f(0) = 0$. In addition, $f'(0) = 0$. The easiest way to see this is to note that, among the terms in $f'(k)$, the only one that can possibly be nonzero at $k=0$ is the one for which the derivative acts on the k in the numerator of the fraction in Eq. (A13). Thus,

$$f'(0) = \int dp\, d\phi\, d\theta \sin\theta \sin\phi\, \mathrm{e}^{-p^2/\Lambda^2} = 0, \tag{B4}$$

as the angular integrals vanish by symmetry. Clearly, we must consider $f''(0)$. A direct evaluation of $f''(0)$ does indeed yield a finite result, so that the leading contribution comes from the third term in Eq. (B2). Evaluating the integral over k in this term then yields $\delta\lambda_c(T) \propto T^3$ for $T\to 0$ yielding the first line of Eq. (19).

Next, we turn to the $\varepsilon_{\rm c}$ dependence of $\lambda_c^{-2}(0)$. It is simplest to consider the scaled function $I_2(\varepsilon_{\rm c},\eta)$, which may be written as

$$I_2(\varepsilon_{\rm c},1) \;=\; \int d^2k \int d^2p\, \frac{k_2 p_2}{kp}\frac{1}{k+p} \mathrm{e}^{-k^2/\varepsilon_{\rm c}^2} \mathrm{e}^{-p^2/\varepsilon_{\rm c}^2} \times \mathrm{e}^{-(\mathbf{k}-\mathbf{p})^2}. \tag{B5}$$

Equation (B5) is obtained from Eq. (23b) by replacing the integrals over the unit disk with a smooth Gaussian cutoff and then rescaling $\mathbf{k}\to\mathbf{k}/\varepsilon_{\rm c}$ (and similarly for $\mathbf{p}$). We have also set $\eta = 1$ for convenience. We proceed in the same manner as for the case of $\delta\lambda_c(T)$ above, writing $I_2(\varepsilon_{\rm c},1)$ as

$$\begin{aligned} I_2(\varepsilon_{\rm c},1) \;&=\; \int_0^\infty dk g(k) \mathrm{e}^{-k^2/\varepsilon_{\rm c}^2}, &(B6)\\ &\approx \int_0^\infty dk[g(0)+kg'(0)+\cdots]\mathrm{e}^{-k^2/\varepsilon_{\rm c}^2}, &(B7)\\ g(k) \;&\equiv \int p\, dp\, d\phi\, d\theta \frac{k\sin\theta\sin\phi}{k+p} \mathrm{e}^{-p^2/\varepsilon_{\rm c}^2} \times \mathrm{e}^{-(\mathbf{k}-\mathbf{p})^2}. &(B8)\end{aligned}$$

Owing to the fact that the Gaussian function is sharply peaked near $k=0$, we have in Eq. (B7) approximately evaluated Eq. (B6) by Taylor expanding $g(k)$ in analogy with Eq. (B2). As in the previous case, $g(0)=0$ and $g'(0)=0$, requiring the evaluation of $g''(0)$. Thus, the calculation proceeds exactly as above, with one important difference: The function $g(k)$ contains a factor $\mathrm{e}^{-p^2/\varepsilon_{\rm c}^2}$ in the integrand. It is straightforward to verify that the integration over p then gives $g''(0) \propto \varepsilon_{\rm c}^2$. Combining this with a factor of $\varepsilon_{\rm c}^3$ arising from the third term in Eq. (B7), we have that $I_2(\varepsilon_{\rm c},1) \propto \varepsilon_{\rm c}^5$ for $\varepsilon_{\rm c}\to 0$, immediately giving the first line of Eq. (20).

* Present address: Department of Physics, University of Colorado, Boulder, CO 80309, USA

[1] P. W. Anderson, *The theory of superconductivity in the high-T_c cuprates*, Princeton University Press (1997).
[2] V. J. Emery and S. A. Kivelson, Nature **374**, 434 (1995).
[3] S.C. Zhang, Science **275**, 1089 (1997).
[4] L. Balents, M. P. A. Fisher and C. Nayak, Phys. Rev. B **60**, 1654 (1999).
[5] M. Franz and Z. Tešanović, Phys. Rev. Lett. **87**, 257003 (2001).
[6] Y. J. Uemura, G. M. Luke, B. J. Sternlieb, J. H. Brewer, J. F. Carolan, W. N. Hardy, R. Kadono, J. R. Kempton, R. F.

Kiefl, S. R. Kreitzman, P. Mulhern, T. M. Riseman, D. Ll. Williams, B. X. Yang, S. Uchida, H. Takagi, J. Gopalakrishnan, A. W. Sleight, M. A. Subramanian, C. L. Chien, M. Z. Cieplak, Gang Xiao, V. Y. Lee, B. W. Statt, C. E. Stronach, W. J. Kossler, and X. H. Yu, Phys. Rev. Lett **62**, 2317 (1989).

[7] T. Timusk and B.W. Statt, Rep. Prog. Phys. **62**, 61 (1999).

[8] Ruixing Liang, D.A. Bonn, W.N. Hardy, J.C. Wynn, K.A. Moler, L. Lu, S. Larochelle, L. Zhou, M. Greven, L. Lurio and S.G.J. Mochrie, Physica C **383**, 1 (2002).

[9] A. Hosseini, *The anisotropic microwave electrodynamics of YBCO*, Ph.D. Thesis, University of British Columbia (2002).

[10] A. Hosseini, D.M. Broun, D.E. Sheehy, T.P. Davis, M. Franz, W.N. Hardy, Ruixing Liang, and D.A. Bonn, submitted to Phys. Rev. Lett. (2003).

[11] L.B. Ioffe and A.J. Millis, J. Phys. Chem. Solids **63**, 2259 (2002).

[12] D.A. Bonn, S. Kamal, A. Bonakdarpour, Ruixing Liang, W.N. Hardy, C.C. Homes, D.N. Basov, and T. Timusk, Czech. J. Phys. **46**, 3195 (1996).

[13] B.R. Boyce, J.A. Skinta, and T.R.Lemberger, Physica C 341, 561-562 (2000); B.R. Boyce, K.M. Paget, T.R. Lemberger, cond-mat/9907196.

[14] P.A. Lee and X.-G. Wen, Phys. Rev. Lett. **78**, 4111 (1997).

[15] T. Pereg-Barnea, P.J. Turner, R. Harris, G.K. Mullins, J.S. Bobowski, M. Raudsepp, R. Liang, D.A. Bonn and W.N. Hardy, cond-mat/0311555.

[16] See however Ref. 15 which suggests doping dependence closer to x^2 in moderately underdoped YBCO single crystals.

[17] D.J. Scalapino, Phys. Rep. **250**, 329 (1995)

[18] M. Sutherland, D.G. Hawthorn, R.W. Hill, F. Ronning, S. Wakimoto, H. Zhang, C. Proust, E. Boaknin, C. Lupien, L. Taillefer, R. Liang, D.A. Bonn, W.N. Hardy, R. Gagnon, N.E. Hussey, T. Kimura, M. Nohara, H. Takagi, cond-mat/0301105.

[19] P.W. Anderson, Science **235**, 1169 (1987).

[20] A. Paramekanti, M. Randeria and N. Trivedi, Phys. Rev. Lett. **87**, 217002 (2001).

[21] R.B. Laughlin, cond-mat/0209269.

[22] A. Hosseini, Saeid Kamal, D.A. Bonn, Ruixing Liang, and W.N. Hardy, Phys. Rev. Lett. **81**, 1298 (1998).

[23] C. Panagopoulos, T. Xiang, W. Anakool, J.R. Cooper, Y.S. Wang, C.W. Chu, Phys. Rev. B **67**, 220502 (2003).

[24] R.J. Radtke, V.N. Kostur and K. Levin, Phys. Rev. B **53**, R522 (1996).

[25] R.J. Radtke and V.N. Kostur, Can. J. Phys. **75**, 363 (1997).

[26] T. Xiang and J. M. Wheatley, Phys. Rev. Lett. **77**, 4632 (1996).

[27] A.J. Millis, S.M. Girvin, L.B. Ioffe and A.I. Larkin, J. Phys. Chem. Solids **59**, 1742 (1998).

[28] D. J. Scalapino, S. R. White, and S. Zhang, Phys. Rev. B **47**, 7995 (1993).

[29] Q.-H. Wang, J.H. Han, and D.-H. Lee, Phys. Rev. Lett. **87**, 077004 (2001).

[30] A.C. Durst and P.A. Lee, Phys. Rev. B **62**, 1270 (2000).

[31] H. Ding, M. R. Norman, T. Yokoya, T. Takeuchi, M. Randeria, J.C. Campuzano, T. Takahashi, T. Mochiku, and K. Kadowaki, Phys. Rev. Lett. **78**, 2628 (1997).

[32] Ch. Renner, B. Revaz, J.-Y. Genoud, K. Kadowaki and Ø. Fischer, Phys. Rev. Lett. **80**, 149 (1998).

[33] We are indebted to P.A. Lee for pointing out this possibility to us.

[34] See, e.g., G.D. Mahan, *Many Particle Physics* (Plenum, New York, 1990).

[35] See, e.g., M. Tinkham, *Introduction to Superconductivity*, McGraw-Hill, 1996.

[36] K.M. Lang, V. Madhavan, J.E. Hoffman, E.W. Hudson, H. Eisaki, S. Uchida and J.C. Davis, Nature **415**, 412 (2002).

[37] M.R. Norman, H. Ding, M. Randeria, J.C. Campuzano, T. Yokoya, T. Takeuchi, T. Takahashi, T. Mochiku, K. Kadowaki, P. Guptasrma and D.G. Hinks, Nature **392**, 157 (1998).

[38] P.A. Lee and X.-G. Wen, private communication.

[39] M.B. Walker, Phys. Rev. B **64**, 134515 (2001).

[40] A. Paramekanti and M. Randeria, Phys. Rev. B **66**, 214517 (2002).

[41] M. Vojta, Y. Zhang, and S. Sachdev, Phys. Rev. B **62**, 6721 (2000).

[42] S. Chakravarty, R.B. Laughlin, D.K. Morr, and C. Nayak Phys. Rev. B **63**, 094503 (2001).

[43] S. Tewari, H.-Y. Kee, C. Nayak, and S. Chakravarty, Phys. Rev. B **64**, 224516 (2001).

[44] H.-Y.Kee and Y.-B. Kim, Phys. Rev. B **66**, 052504 (2002).